



Swansea University
Prifysgol Abertawe



Cronfa - Swansea University Open Access Repository

This is an author produced version of a paper published in:
Global Ecology and Biogeography

Cronfa URL for this paper:
<http://cronfa.swan.ac.uk/Record/cronfa51038>

Paper:

Shestakova, T., Voltas, J., Saurer, M., Berninger, F., Esper, J., AndreuHayles, L., Daux, V., Helle, G., Leuenberger, M., et. al. (2019). Spatiotemporal patterns of tree growth as related to carbon isotope fractionation in European forests under changing climate. *Global Ecology and Biogeography*
<http://dx.doi.org/10.1111/geb.12933>

This item is brought to you by Swansea University. Any person downloading material is agreeing to abide by the terms of the repository licence. Copies of full text items may be used or reproduced in any format or medium, without prior permission for personal research or study, educational or non-commercial purposes only. The copyright for any work remains with the original author unless otherwise specified. The full-text must not be sold in any format or medium without the formal permission of the copyright holder.

Permission for multiple reproductions should be obtained from the original author.

Authors are personally responsible for adhering to copyright and publisher restrictions when uploading content to the repository.

<http://www.swansea.ac.uk/library/researchsupport/ris-support/>

1 **Spatiotemporal patterns of tree growth as related to carbon isotope fractionation in**
2 **European forests under changing climate**

3

4 **Running head:** Ecophysiology of forest growth in Europe

5

6 Tatiana A. Shestakova^{1,2}, Jordi Voltas², Matthias Saurer³, Frank Berninger⁴, Jan Esper⁵, Laia
7 Andreu-Hayles⁶, Valérie Daux⁷, Gerhard Helle⁸, Markus Leuenberger⁹, Neil J. Loader¹⁰,
8 Valérie Masson-Delmotte⁷, Antonio Saracino¹¹, John S. Waterhouse¹², Gerhard H. Schleser¹³,
9 Zdzisław Bednarz¹⁴, Tatjana Boettger¹⁵, Isabel Dorado-Liñán¹⁶, Marc Filot^{9†}, David Frank¹⁷,
10 Michael Grabner¹⁸, Marika Haupt¹⁵, Emmi Hilasvuori¹⁹, Högne Jungner¹⁹, Maarit Kalela-
11 Brundin²⁰, Marek Krąpiec²¹, Hamid Marah²², Sławomira Pawełczyk²³, Anna Pazdur²³,
12 Monique Pierre⁷, Octavi Planells²⁴, Rūtilė Pukienė²⁵, Christina E. Reynolds-Henne²⁶, Katja T.
13 Rinne²⁷, Angelo Rita²⁸, Eloni Sonninen¹⁹, Michel Stiévenard⁷, Vincent R. Switsur^{12‡}, Elżbieta
14 Szychowska-Krąpiec²¹, Malgorzata Szymaszek^{23§}, Luigi Todaro²⁸, Kerstin Treydte³, Adomas
15 Vitas²⁹, Martin Weigl³⁰, Rupert Wimmer³¹, Emilia Gutiérrez^{24*}

16

17 ¹ Woods Hole Research Center, Falmouth, MA, USA

18 ² Department of Crop and Forest Sciences – AGROTECNIO Center, University of Lleida,
19 Lleida, Spain

20 ³ Swiss Federal Research Institute WSL, Birmensdorf, Switzerland

21 ⁴ Department of Forest Sciences, University of Helsinki, Helsinki, Finland

22 ⁵ Department of Geography, Johannes Gutenberg University, Mainz, Germany

23 ⁶ Tree-Ring Laboratory, Lamont-Doherty Earth Observatory of Columbia University,
24 Palisades, USA

25 ⁷ Laboratory for Climate and Environmental Sciences, CEA/CNRS/UVSQ, Gif-sur-Yvette,
26 France

27 ⁸ Helmholtz-Centre Potsdam, German Centre for Geosciences – GFZ, Potsdam, Germany

28 ⁹ Climate and Environmental Physics, University of Bern, Bern, Switzerland

29 ¹⁰ Department of Geography, Swansea University, Swansea, UK

30 ¹¹ Department of Agricultural Sciences, University of Naples Federico II, Portici, Italy

31 ¹² Department of Biomedical and Forensic Sciences, Anglia Ruskin University, Cambridge,
32 UK

33 ¹³ FZJ Research Center Jülich, Institute of Bio- and Geosciences IBG-3, Jülich, Germany

34 ¹⁴ Department of Forest Biodiversity, Agricultural University, Krakow, Poland

- 35 ¹⁵ Department of Isotope Hydrology, Helmholtz Centre for Environmental Research – UFZ,
36 Halle, Germany
- 37 ¹⁶ Forest Research Centre, National Institute for Agricultural Research and Experimentation
38 (INIA-CIFOR), Madrid, Spain
- 39 ¹⁷ Laboratory of Tree-Ring Research, University of Arizona, Tucson, USA
- 40 ¹⁸ Institute of Wood Technology and Renewable Resources, University of Natural Resources
41 and Life Sciences – BOKU, Vienna, Austria
- 42 ¹⁹ Laboratory of Chronology, University of Helsinki, Helsinki, Finland
- 43 ²⁰ Forestry Museum, Lycksele, Sweden
- 44 ²¹ Faculty of Geology, Geophysics and Environmental Protection, AGH University of Science
45 and Technology, Krakow, Poland
- 46 ²² Water and Climate Unit, CNESTEN, Rabat, Morocco
- 47 ²³ Department of Radioisotopes, Silesian University of Technology, Gliwice, Poland
- 48 ²⁴ Department of Biological Evolution, Ecology and Environmental Sciences, University of
49 Barcelona, Barcelona, Spain
- 50 ²⁵ Nature Research Centre, Institute of Geology and Geography, Vilnius, Lithuania
- 51 ²⁶ Oeschger Centre for Climate Change Research, University of Bern, Bern, Switzerland
- 52 ²⁷ Natural Resources Institute Finland (Luke), Vantaa, Finland
- 53 ²⁸ School of Agricultural, Forest, Food and Environmental Sciences, University of Basilicata,
54 Potenza, Italy
- 55 ²⁹ Environmental Research Centre, Vytautas Magnus University, Kaunas, Lithuania
- 56 ³⁰ Holzforschung Austria, Vienna, Austria
- 57 ³¹ Institute for Natural Materials Technology, University of Natural Resources and Life
58 Sciences, Tulln, Austria
- 59 † Present address: CSL Behring AG, Bern, Switzerland
- 60 ‡ Deceased
- 61 § Present address: Janusz Kusocinski Sports School in Zabrze, Zabrze, Poland
- 62
- 63 *Corresponding author: Emilia Gutiérrez
64 Tel: +34 934037143
65 Email: emgutierrez@ub.edu
66
67

68 **Acknowledgements**

69 T.A.S. acknowledges the ERANET-Mundus program (European Commission, Grant
70 agreement 20112573), the COST Action FP1304 via the STSM program (European
71 Commission, COST-STSM-ECOST-STSM-FP1304-140915-066395), and the Spanish
72 Government (grant number AGL2015-68274-C3-3-R). This study was supported by the EU-
73 project ISONET (EVK2-2001-00237). We are also grateful to Carmela Miriam D'Alessandro,
74 Nathalie Etien, Marie-Thérèse Guillemin and Werner Laumer for field and laboratory
75 assistance.

76 **Abstract**

77 *Aim*

78 To decipher continent-wide spatiotemporal patterns of forest growth dynamics and their
79 associations with carbon isotope fractionation processes inferred from tree rings as modulated
80 by climate warming in Europe.

81

82 *Location*

83 Europe and North Africa (30–70°N, 10°W–35°E).

84

85 *Time period*

86 1901–2003.

87

88 *Major taxa studied*

89 Temperate and Euro-Siberian trees.

90

91 *Methods*

92 We characterize changes in the relationship between tree productivity and carbon isotope
93 fractionation over the 20th century using a European network. Using indexed tree-ring widths
94 (TRW_i), we assess shifts in the temporal coherence of radial growth (synchrony) for five forest
95 ecosystems (Atlantic, Boreal, cold continental, Mediterranean and temperate). We also examine
96 whether TRW_i shows increased coupling with leaf-level gas exchange, inferred from indexed
97 carbon isotope discrimination in tree-ring cellulose ($\Delta^{13}C_i$), through enhanced stomatal
98 regulation in response to amplified drought stress spreading northwards.

99

100 *Results*

101 We find spatial autocorrelation for TRW_i and $\Delta^{13}C_i$ extending over up to 1,000 km among forest
102 stands. However, growth synchrony is not uniform across Europe, but increases along a
103 latitudinal gradient concurrent with decreasing temperature and evapotranspiration.
104 Latitudinally-structured relationships between TRW_i and $\Delta^{13}C_i$ (changing from negative to
105 positive as latitude increased) point to drought impairing carbon uptake via stomatal regulation
106 of water losses as the main mechanism underlying synchronous forest growth in continental
107 Europe below 50°N. At the turn of this century, warming-induced effects on leaf physiology
108 increased synchrony in tree growth among European forests to unprecedented levels over the
109 last century.

110

111 *Main conclusions*

112 Increased growth synchrony from the first to the second half of the 20th century in
113 Mediterranean, temperate and cold continental forests, together with a tighter relationship
114 between TRW_i and $\Delta^{13}\text{C}_i$, indicate increasing drought effects on productivity across Europe.
115 Such recent tendency towards exacerbated moisture-sensitive forest growth could override a
116 positive effect of enhanced leaf intercellular CO₂ concentration, resulting in forthcoming
117 declines in forest carbon gain continent-wide.

118

119

120 **Keywords:** carbon isotopes, climate change, dendroecology, drought stress, European forests,
121 latitudinal gradients, *Pinus*, *Quercus*, stomatal control, tree rings

122 **Introduction**

123 Understanding the physiological mechanisms underlying variations in forest productivity is a
124 key priority in global change research. Factors such as tree age, forest structure and
125 management, nutrient availability, pollution and disturbance regimes influence the carbon
126 budget of forested areas. During the last decades, however, climate change and increased
127 atmospheric CO₂ (atmCO₂) have largely altered the growth of natural forests (Nabuurs et al.,
128 2013). To explore these dynamics, research efforts have been mainly confined to local
129 ecosystems, with some representative woody species and their interactions examined at small
130 spatial scales (Pivovarov et al., 2016). This approach is hampered by site-dependent effects and
131 limited representativeness of environmental conditions. A comprehensive understanding of tree
132 functioning is urgently needed across broad regions in order to assess the potential and limits
133 of forest carbon uptake globally (Chown, Gaston, & Robinson, 2004). Through the analysis of
134 meaningful functional traits (Violle, Reich, Pacala, Enquist, & Kattge, 2014), the interpretation
135 of spatiotemporal patterns of forest growth variability can provide comprehensive insights into
136 the environmental responses that may change forest's services for carbon storage in the next
137 decades (Anderegg et al., 2016).

138 The mechanisms and processes influencing forest productivity are extremely variable
139 (Gibert, Gray, Westoby, Wright, & Falster, 2016). Despite such complexity, regionally
140 coherent multispecies responses have been linked to global change effects on forest ecosystems
141 using tree-ring networks (Babst et al., 2013; Shestakova et al., 2016). Dendroecological studies
142 rely on the presence of common signals archived in tree populations, which are often derived
143 from ring-width series reflecting variations in environmental factors (Fritts, 2001).
144 Alternatively, stable isotopes are proxies of ecophysiological traits that are valuable to assess
145 plant carbon and water relations at large spatiotemporal scales (Werner et al., 2012; Frank et
146 al., 2015). In particular, the carbon isotope discrimination ($\Delta^{13}\text{C}$) of tree rings reflect more
147 directly the complex array of physiological responses to environmental conditions than classical
148 dendrochronological traits such as ring-width (Treydte et al., 2007; Gessler et al., 2014). The
149 ratio of the heavy to light carbon isotopes ($^{13}\text{C}/^{12}\text{C}$) of organic matter depends on factors
150 affecting CO₂ assimilation, which is mainly controlled by photosynthetic rate (A) and stomatal
151 conductance (g_s) (Farquhar, Ehleringer, & Hubick 1989). Hence, the interannual variation in
152 $\Delta^{13}\text{C}$ can be evaluated and retrospectively related to leaf-level physiological processes (e.g.,
153 Andreu-Hayles et al., 2011; Shestakova, Aguilera, Ferrio, Gutiérrez, & Voltas, 2014). This is
154 especially relevant in temperate forests thriving under near-optimal conditions, where tree
155 growth patterns may not be informative of climate variability, but stable isotopes have been

156 shown to be sensitive to environmental variables (Hartl-Meier et al., 2015). Indeed, much
157 complementary information can be gained by analysing carbon isotopes in addition to ring-
158 widths (Cernusak & English, 2015), which together provide relevant evidence on how trees
159 respond to climate change and increasing atmCO_2 (Andreu-Hayles et al., 2011; Saurer et al.,
160 2014).

161 In drought-prone environments, tree-ring $\Delta^{13}\text{C}$ can be mainly related to the stomatal
162 control of CO_2 fluxes into the leaf, integrating any environmental variable affecting stomatal
163 conductance (Gessler et al., 2014). Under such conditions, radial growth and $\Delta^{13}\text{C}$ are bound
164 together by two factors: stomatal regulation and water availability. However, $\Delta^{13}\text{C}$ is also
165 affected by changes in photosynthetic activity associated with irradiance, phenology, nutritional
166 stresses or N deposition when water becomes less limiting (Livingston et al., 1998). By
167 combining ring-width and $\Delta^{13}\text{C}$, information can be gained on the array of tree performances
168 that underlie biogeographical interactions, as these traits share spatial responses to drought
169 events (Voelker, Meinzer, Lachenbruch, Brooks, & Guyette, 2014).

170 In the present study, we attempt to characterize the degree of dependence of stem growth
171 on photosynthetic carbon isotope fractionation across European forests using a unique tree-ring
172 network (Treydte et al., 2007). So far, only the isotope data of this network have been analysed,
173 but not radial growth, nor the relationship between the two parameters. We used 20
174 chronologies from old trees comprising conifers (*Pinus*) and oaks (*Quercus*) spanning the 20th
175 century and ranging from Mediterranean to Boreal latitudes (37°N to 69°N). Indeed, latitudinal
176 gradients are extremely relevant for the analysis of large-scale patterns of trait variability and
177 their relationships with ecosystem functioning (Violle et al., 2014). We hypothesise that, on a
178 continental scale, (i) the temporal coherence of radial growth in forest trees is geographically
179 structured, with more synchronous growth to be found among cold-limited, high latitude forests
180 than among drought-prone, low-latitude forests (Shestakova et al., 2016); (ii) these patterns of
181 synchrony are linked to the relative significance of carbon assimilation and stomatal control on
182 growth determination, as reflected by relationships between ring-widths and $\Delta^{13}\text{C}$; and (iii)
183 warming-induced drought stress triggers a tighter stomatal control of water losses which, in
184 turn, enhances synchrony in low latitude forests owing to more coordinated physiological
185 reactions to climate. On the basis of the joint analysis of radial growth and $\Delta^{13}\text{C}$, the assessment
186 of spatiotemporal tree responses to environmental changes may improve our understanding of
187 growth and physiology changes experienced by European forests throughout the 20th century.

188
189

190 **Materials and methods**

191 *Tree-ring network*

192 We used a tree-ring dataset from the pan-European network ISONET (European Union, EVK2-
193 2001-00237), which is comprised of 20 sites and provides a comprehensive coverage of the
194 biogeographic conditions that are found across Europe into northern Africa (Treydte et al.,
195 2007) (Table 1). Sites consist of old-grown forests (mean age = 454 ± 196 years [SD]) from the
196 two main genera in Europe (*Pinus* and *Quercus*) plus *Cedrus atlantica* (Morocco). The forests
197 originate from semiarid (Mediterranean basin), humid temperate (western-central Europe), cold
198 continental (north-central Europe) and subarctic (Fennoscandia) climates (Table 1). The
199 sampled trees are temperate (*Quercus petraea*, *Q. robur*) and Euro-Siberian (*Pinus nigra*, *P.*
200 *sylvestris*, *P. uncinata*) taxa, with sites distributed across most of their climatic ranges (Table 1).
201 Sampled stands spread along broad latitudinal (from 32°58'N to 68°56'N) and altitudinal (from
202 5 m to 2,100 m a.s.l.) gradients, with high-elevation sites concentrated in southern Europe.
203 Conifers are the dominant species in unmanaged cold Boreal or Mediterranean zones (i.e., high-
204 latitude or high-elevation sites), whereas oaks are mainly found in humid western and central
205 European lowlands. The distance between sites varies from about 50 km up to 4,500 km.

206 Increment cores were extracted from numerous trees at each site (Table S1), and tree
207 rings were cross-dated and measured following standard dendrochronological procedures
208 (Cook & Kairiukstis, 1990). As a proxy for above-ground woody biomass accumulation, basal
209 area increment (BAI) for each stand was calculated as the bi-weight site mean of BAI of
210 individual ring-width series. Temporal trends in the BAI chronologies were estimated through
211 the slope (b) of the linear regression of BAI records on time. Indexed tree-ring width (TRW_i)
212 and carbon isotope discrimination ($\Delta^{13}C_i$) chronologies were obtained by high-pass filtering
213 and autocorrelation removal (see Appendix 1 in Supporting Information). Details on tree-ring
214 network characteristics can be found in Appendix 2. The indexed ring-width and isotope
215 chronologies were used as input for statistical analyses. The study period was 1901–2003.

216

217 *Analysis of spatial variability of tree growth*

218 Spatial structure of tree-ring traits and climatic signals across Europe

219 The temporal coherence of tree-ring signals (TRW_i , $\Delta^{13}C_i$) among sites was characterized to
220 determine how far such coherence extends over Europe. To this end, correlation coefficients (r)
221 between pairs of chronologies, calculated over the period 1901–2003, were regressed on their
222 geographic distance using a negative exponential function for both TRW_i and $\Delta^{13}C_i$. The
223 modified correlogram technique (Koenig & Knops, 1998) was also employed to characterize

224 the spatial autocorrelations in the network. To this end, the statistical significance of the
225 pairwise correlations among chronologies was calculated within classes located 500 km apart.
226 Chronologies located farther than 2,500 km apart were combined into a single class. Hence, six
227 classes were defined ranging from <500 to >2,500 km. To evaluate the geographic extent of
228 synchrony in climate factors, the same analysis was performed for mean annual temperature
229 and precipitation.

230

231 Temporal coherence of ring-width signals

232 The investigation of common TRW_i variability among chronologies (growth synchrony, \hat{a}) was
233 performed through variance-covariance (VCOV) modelling following Shestakova et al. (2014,
234 2018) (Appendix 3.1). This approach is suited to test the presence of contrasting tree-ring
235 patterns in pre-established groups of chronologies, where particular groups can be defined
236 based on existing knowledge (Shestakova et al., 2018). Here, the 20 chronologies were
237 classified into four groups according to membership to a particular climate type following the
238 Köppen climate classification (Köppen & Geiger, 1936): Boreal (*Dfc*), cold continental (*Dfb*),
239 humid temperate (*Cfb*) and Mediterranean (*Csb*) (Table 1). In turn, the humid temperate climate
240 was split into Atlantic (for western Europe chronologies) and temperate (for central Europe
241 chronologies) types. These two groups originated as the result of constraining the maximum
242 distance among sites at the group level to 1,000 km (i.e., the spatial range of coherent tree-ring
243 signals as inferred from correlograms). Therefore, five different groups were defined. Each
244 group consisted of a number of neighbouring forest stands (≥ 3) that ensured a solution to mixed
245 model estimates.

246 A number of variance-covariance (VCOV) models accommodating between- and
247 within-group variability were tested and compared using Akaike and Bayesian information
248 criteria for model selection, which favour parsimonious models (Burnham & Anderson, 2002).
249 The VCOV models were broad evaluation (denoting common synchrony across groups),
250 narrow evaluation (corresponding to a banded main diagonal matrix denoting perfect
251 asynchrony between groups), unstructured (a completely general covariance matrix),
252 compound symmetry (a matrix having constant variance and covariance) and variants of a
253 Toeplitz structure (a matrix allowing for different (co)variances depending on the relative
254 proximity or neighbourhood among groups). These models are described in detail in Table S2.
255 Afterwards, estimates of growth synchrony (\hat{a}) were derived using the best VCOV model for
256 the entire period (1901–2003) (Shestakova et al., 2018). The evolution of changes in \hat{a} was also
257 studied for successive 50-year segments lagged one year by fitting the same VCOV models.

258 The best fitting model was independently selected for each segment. This was done to
259 characterise shifts in common TRW_i variability over time potentially related to instability in
260 the relationship between tree growth and climate factors at the high-frequency domain.
261 Significant trends were determined by using the non-parametric Kendall τ rank correlation
262 coefficient.

263

264 Relationships between radial growth and carbon isotope discrimination

265 The temporal (yearly) association between TRW_i and $\Delta^{13}C_i$ (hereafter, r_Y) was investigated at
266 the group level through a bivariate mixed-effects model (Appendix 3.2) (Shestakova et al.,
267 2017). Broadly speaking, this approach estimates the extent by which TRW_i and $\Delta^{13}C_i$,
268 measured on the same set of chronologies, contain overlapping information as a result of plant
269 processes related to carbon uptake and water use. Hence, the relevance of a physiological
270 attribute ($\Delta^{13}C_i$) as determinant of regional forest growth is quantified by estimating how much
271 of TRW_i variability across chronologies is associated with the variability of isotopic records.
272 We argue that this quantification is relevant for studying the variable role of a putative
273 physiological tracer of productivity across large areas. The bivariate analysis was performed
274 for the entire period (1901–2003). We also evaluated the changes in r_Y between TRW_i and $\Delta^{13}C_i$
275 chronologies for successive 50-year segments lagged one year.

276

277 *Meteorological data*

278 Monthly mean temperature, precipitation and potential evapotranspiration were used for
279 climate characterization. Meteorological variables were obtained from the nearest grid point to
280 each site of the high-resolution climate dataset (Climatic Research Unit, CRU TS 3.21; Harris,
281 Jones, Osborn, & Lister, 2014). CRU provides climate series on a $0.5^\circ \times 0.5^\circ$ grid-box basis,
282 interpolated from meteorological stations across the globe, and extends back to 1901. However,
283 it should be noted that climate data mainly originate from low-elevation stations. This leads to
284 remarkable differences in elevation between stations and sampling sites in mountainous
285 Mediterranean areas. To account for this discrepancy, we applied lapse rate adjustments to the
286 CRU dataset for the Mediterranean sites ($<45^\circ N$) following Gandullo (1994). Potential
287 evapotranspiration was estimated from CRU records using the Hargreaves method (Hargreaves
288 & Samani, 1982).

289 Bootstrapped correlations between TRW_i or $\Delta^{13}C_i$ chronologies and monthly
290 temperature, precipitation and the Standardized Precipitation-Evapotranspiration Index (SPEI3,
291 a 3-month integrated drought index; Vicente-Serrano, Beguería, & López-Moreno, 2010) were

292 computed over the period 1901–2003 to examine site-specific responses to climate. To assess
293 the temporal stability of these responses, the same analysis was conducted for the split 1901–
294 1950 and 1951–2003 periods. To ensure that results were driven by local climate rather than by
295 long-term trends (e.g., global warming), the climatic series exhibiting a linear trend over time
296 were detrended by fitting a straight line and keeping the residuals of these linear fits or,
297 otherwise, simply differencing from the mean. Climate relationships were analysed from the
298 previous October to the current September of tree-ring formation.

299

300 *Analysis of biogeographical patterns of tree performance*

301 To characterize the spatial patterns of tree growth and its dependence on $\Delta^{13}\text{C}$, changes in
302 growth synchrony (\hat{a}) and in the relationship between TRW_i and $\Delta^{13}\text{C}_i$ (r_Y) were evaluated as a
303 function of biophysical variables through simple correlations. We used geographic (latitude,
304 longitude and elevation) and climatic records (mean annual temperature [MAT], mean annual
305 precipitation [MAP] and potential evapotranspiration [PET]; period 1901–2003) averaged
306 across sites for every group. It should be noted that climatic records in the network strongly
307 depended on geographic location: MAT decreased linearly with increasing latitude ($r = -0.61$,
308 $P < 0.01$) and longitude (or distance inland from the Atlantic Sea) ($r = -0.50$, $P < 0.05$), but it
309 was not related to elevation. Similarly, PET was negatively related to latitude ($r = -0.84$,
310 $P < 0.001$) and longitude ($r = -0.58$, $P < 0.01$), and positively to elevation ($r = 0.45$, $P < 0.05$).
311 MAP was also positively related to elevation ($r = 0.45$, $P < 0.05$). The stability of these
312 relationships was assessed through correlation analysis for the split 1901–1950 and 1951–2003
313 periods.

314

315 **Results**

316 *Site-level growth trends and responses to climate*

317 Eleven sites showed positive BAI trends and one site showed a negative BAI trend (slope b ,
318 $P < 0.05$) for the period 1901–2003, while no significant trend was detected for seven sites
319 (Table 1). Growth acceleration was observed at all oak sites and at three pine sites from mid
320 and high latitudes, whereas growth significantly declined in a Mediterranean site. High summer
321 temperatures enhanced growth in Fennoscandia, whereas summer drought often constrained
322 growth at central and southern latitudes (as indicated by negative correlations with summer
323 temperature and positive correlations with summer precipitation and SPEI3) (Fig. S1a–c). In
324 addition, the positive growth responses to high winter temperatures observed at some mid- and
325 low-latitude sites suggested co-limitation by cold winters and dry summers. In comparison,

326 more clear-cut climate signals were shared by $\Delta^{13}\text{C}_i$ records, which were especially associated
327 with summer temperatures (negatively) and summer precipitation and SPEI3 (positively)
328 (Fig. S1d–f).

329

330 *Spatial consistency of tree-ring signals*

331 Naturally, the correlations between pairs of chronologies for TRW_i decreased with increasing
332 distance between sites. This effect accounted for 29% variability of inter-site correlation
333 coefficients if subject to exponential decay (Fig. 1a). The highest correlations were found
334 between *Quercus* stands from central Europe and between *Pinus* stands from north-eastern
335 Europe ($r \geq 0.30$). Significant spatial autocorrelation was recorded up to 1,000 km, with a mean
336 correlation of 0.22 and 0.12 for sites within distances of 0–500 and 501–1,000 km, respectively
337 (Fig. 1c). A Principal Component Analysis performed on TRW_i returned five principal
338 components (PCs) that accounted for 50% of the total variance. The first PC, which explained
339 12.9% of variance, had positive loadings for all chronologies, except for one Iberian site with
340 *P. sylvestris* and the Moroccan site with *C. atlantica* (Fig. S2). The highest PC1 loadings
341 corresponded to western and central European chronologies, indicating larger growth
342 similarities compared to peripheral chronologies, located farther away from each other. The
343 second PC, which explained 11.0% of variance, was also related to the geographic location of
344 chronologies: positive PC2 loadings corresponded to south-western chronologies, while north-
345 eastern chronologies had negative loadings (Fig. S2). The remaining three PCs accounted for
346 <10% of variance and showed mixed spatial signals, indicating species-specific differences and
347 the influence of local conditions on tree growth.

348 For $\Delta^{13}\text{C}_i$ chronologies, we found an exponential decrease in coherence with distance
349 between chronology pairs accounting for 28% variability of inter-site correlation coefficients
350 (Fig. 1b). Significant spatial autocorrelations were recorded up to 1,000 km (Fig. 1d). Similarly,
351 the analysis of spatial autocorrelation in climate parameters revealed that the common signal
352 declined with distance (Fig. S3a,b) and extended >2,500 km for MAT (linear function) and up
353 to 1,000 km for MAP (decay function) (Fig. S3c,d). There was also a significant negative
354 association between the most distant sites (>2,500 km) for MAP.

355

356 *Tree growth synchrony across Europe*

357 The five climate groups identified across the network consisted of three to five chronologies
358 sharing temporal growth patterns (Fig. 2). A heterogeneous Toeplitz with two bands was the
359 best model for the period 1901–2003, indicating covariation between neighbouring groups only

360 (Table S3). Growth synchrony (\hat{a}) varied considerably among groups, ranging from 0.06 ± 0.01
361 (Mediterranean) to 0.36 ± 0.06 (Boreal) (mean \pm SE) (Fig. 3a). The \hat{a} values were unrelated to
362 the average distance between sites at the group level, with groups showing the lowest and
363 highest \hat{a} having inter-site distances of 785 ± 118 km and 913 ± 119 km (mean \pm SE),
364 respectively. In addition, the variable number of chronologies at the group level did not
365 influence \hat{a} . At the between-group level, the highest \hat{a} was found between Boreal and cold
366 continental forests (0.11 ± 0.02), with progressively decreasing common signals between
367 neighbours observed southwards (Fig. 3b).

368 Differences in synchrony among groups were geographically structured and related to
369 latitude ($r = 0.96$, $P < 0.01$) and longitude ($r = 0.89$, $P < 0.05$), but not to elevation (Fig. S4). At
370 the site level, however, there were strong associations between latitude and longitude ($r = 0.65$,
371 $P < 0.01$), latitude and elevation ($r = -0.59$, $P < 0.01$), and longitude and elevation ($r = -0.44$,
372 $P < 0.10$). To check for geographic consistency in these synchrony gradients across Europe, we
373 examined an independent, larger dataset of ring-width chronologies obtained from the
374 International Tree-Ring Data Bank (Grissino-Mayer & Fritts, 1997) having the same species
375 representation ($n = 80$; 52 *Pinus* chronologies and 28 *Quercus* chronologies) (Appendix 4). In
376 this case, we also detected a strong latitudinal gradient in \hat{a} (Fig. S5). Consequently, we
377 assumed that this trend was essentially independent of the particular tree-ring network under
378 consideration. The observed geographic gradient in growth synchrony was also analysed in
379 relation to the potential climatic drivers of forest performance across Europe. Notably, climate
380 variables explained most geographic variation in \hat{a} among groups (Fig. S6). We found strong
381 negative relationships between \hat{a} and PET, followed by MAP and MAT, which are consistent
382 with a gradual decrease in evapotranspirative demand and temperature with increasing latitude.

383

384 *Temporal changes in growth synchrony*

385 The synchrony patterns changed markedly across Europe over the 20th century. \hat{a} increased at
386 low and mid latitudes (i.e., in Atlantic, Mediterranean and temperate forests), whereas it
387 decreased at high latitudes (especially in Boreal, but also in cold continental forests) (Fig. 4a).
388 Such divergent geographic trends weakened the relation between \hat{a} and biogeographic factors,
389 resulting in less geographically- and climatically-dependent \hat{a} values across the continent after
390 1950 (Fig. S4, S6). At the between-group level, different trends were observed depending on
391 the particular group combination. For neighbouring groups, we found a substantial decrease in
392 synchrony between Boreal and cold continental forests, whereas synchrony remained steady or
393 increased for other group combinations (Fig. 4b). A modest, albeit sizeable common signal

394 emerged among the more geographically distant group pairs after 1960 ($\hat{a} \approx 0.05-0.10$) (Fig. 4c).
395 In fact, synchrony among forest types strongly converged across Europe in the second half of
396 the century. In contrast, we did not find changes in synchrony patterns of climate parameters
397 (MAT, MAP) throughout the 20th century (results not shown). This led us to discard the
398 possibility that the observed changes in growth synchrony had been driven by concomitant
399 fluctuations in synchrony of climate factors.

400

401 *Tree growth patterns as related to isotopic signals*

402 The temporal variability shared by TRW_i and $\Delta^{13}\text{C}_i$ (r_Y) was investigated at the group level. We
403 found very different, geographically-structured relationships between these traits. The
404 association was mainly positive (for Atlantic, cold-continental and temperate forests) or very
405 positive (for Mediterranean forests), being significantly negative for Boreal forests (Fig. 5),
406 hence following a latitudinal gradient ($r = -0.96$, $P < 0.05$) (Fig. S7). Conversely, r_Y was non-
407 significant for neither longitude nor elevation (Fig. S7). In addition, r_Y was correlated to climate
408 variables at the group level, with the strongest positive association found for both PET and
409 MAP (Fig. S8).

410 The association between TRW_i and $\Delta^{13}\text{C}_i$ changed markedly across Europe throughout
411 the 20th century. r_Y turned from negative to non-significant in Boreal forests, and changed from
412 non-significant to positive in cold-continental (recently), temperate and Mediterranean forests
413 (Fig. 6). As a result, TRW_i and $\Delta^{13}\text{C}_i$ mainly became positively related across Europe. The
414 latitudinal pattern of r_Y was also stronger in the second than in the first half of the century
415 (Fig. S7). This relationship became more dependent on PET after 1950 (Fig. S8).

416

417 **Discussion**

418 This study yields evidence for geographically-structured patterns of forest growth and its
419 associations with carbon isotope fractionation processes across Europe. Common tree growth
420 and physiology were shared by stands spread up to 1,000 km. This outcome provides a general
421 indication on the geographical extent by which climate factors influence tree performance
422 continent-wide; indeed, no other environmental driver is likely to act on the same spatial scale
423 at the high-frequency domain (Fritts, 2001).

424

425 *Geographic structure and climatic controls of tree-ring signals in European forests*

426 Differential growth responses to climate were evident across the network, with temperature-
427 sensitive growth at northern latitudes, precipitation-sensitive growth at central-southern

428 latitudes, and mixed signals in temperate and high-elevation European forests (Babst et al.,
429 2013). Conversely, the extent of common climate signals present in carbon isotopes suggests a
430 tight stomatal control of water losses and, indirectly, photosynthetic activity during summer
431 across most of Europe (Cullen, Adams, Anderson, & Grierson, 2008). These results suggest a
432 partial de-coupling between leaf- and stem-level processes (Jucker et al., 2017). They are
433 consistent with current evidence supporting that carbon allocation patterns change with
434 increasing temperature and this change varies between tree species from different biomes and
435 functional groups (Way & Oren, 2010). Details on the nature and magnitude of carbon isotope
436 signals across the network have been reported by Treydte et al. (2007).

437

438 *Interpreting ring-width patterns continent-wide*

439 Our results show a marked geographical organization of 20th-century growth patterns across
440 Europe. The most conspicuous changes in synchronous tree growth occurred along a north–
441 south gradient, with \hat{a} increasing northwards concurrent with a thermal gradient of decreasing
442 temperature and reduced evapotranspiration (Babst et al., 2013). This agrees with our
443 hypothesis of more synchronous growth in cold-limited, high-latitude forests owing to the
444 greater spatial homogeneity of temperature effects on tree growth in northern Europe (Düthorn,
445 Schneider, Günther, Gläser, & Esper, 2016). It contrasts with the more geographically complex
446 drought events occurring in central and southern Europe (Orlowsky & Seneviratne, 2014),
447 hence resulting in substantially less synchronous growth patterns (Shestakova et al., 2016).

448 Notably, \hat{a} increased after 1950 except in Fennoscandia, which weakened the northward
449 trend of enhanced synchrony observed during the preceding period. This outcome suggests
450 warming-induced climatic forcing spreading across central and southern Europe, irrespective
451 of species and local site conditions, thus enhancing synchrony through common tree sensitivity
452 to such emergent exogenous factor (Fig. S9). It is in line with previous findings on recent high-
453 frequency adjustments of ring-width patterns in response to amplified drought effects on growth
454 in temperate and semiarid regions (Latte, Lebourgeois, & Claessens, 2015; Shestakova et al.,
455 2016). In contrast, climate warming would progressively mitigate low-temperature constraints
456 on tree performance occurring in Boreal forests (Düthorn et al., 2016). This leads to an
457 increasing importance of local (stand-level) effects on tree growth over time, hence triggering
458 regional asynchrony (but see Shestakova et al., 2016). We interpret these phenomena as a sign
459 of increasing drought effects on forest growth dynamics expanding northwards across Europe,
460 which are concurrent with temperature trends across the study area (+0.15 to +0.35°C decade⁻¹
461 between 1960 and 2015) (EEA, 2016).

462

463 *Carbon isotope fractionation relates to spatial patterns of forest growth in Europe*

464 We investigated the physiological mechanisms underlying geographically-structured temporal
465 growth variability through bivariate random-effects modelling of the common temporal signal
466 present in TRW_i and $\Delta^{13}C_i$. This approach is appropriate for investigating exogenous constraints
467 on forest growth and physiology acting over large (continental) climate gradients, because site-
468 level impacts on tree-ring traits (e.g., differential management, competition, soil depth and
469 fertility, etc.) are set aside explicitly from the analysis.

470 The positive relationships between TRW_i and $\Delta^{13}C_i$ at low and mid latitudes suggest
471 that stomatal limitation of leaf carbon assimilation is a key mechanism controlling tree growth
472 synchrony south of 50°N in Europe (Fig. 5). Therefore, leaf-level physiology and tree growth
473 are driven, to a relevant extent, by water stress at about half of the study area (including e.g.,
474 France, Austria and south of Germany and Poland) during the 20th century. Conversely, the
475 negative relationship between TRW_i and $\Delta^{13}C_i$ in Fennoscandia indicates that photosynthesis
476 was constrained by low temperatures/sunshine hours (Gagen et al., 2011). At cool, moist sites
477 the main control over water-use efficiency is assimilation rate, which can be limited by either
478 enzyme activity (photon flux) or enzyme production (leaf temperature or nitrogen availability).
479 These limitations would increase $\Delta^{13}C$ at the expense of decreased carbon uptake, hence
480 reducing radial growth. Although our results must be weighed against the limited spatial
481 representativeness of the sampling network, they allow delineating broad geographical trends
482 that so far have been difficult to ascertain continent-wide, partly due to the unsystematic and
483 sparse nature of data collection (Saurer et al., 2014). Besides, the observed trends agree with
484 previous studies performed across smaller areas showing strong positive ring-width vs. $\Delta^{13}C$
485 correlations for trees growing under water-limited conditions, but weak correlations at wetter
486 and colder sites (Voelker et al., 2014; del Castillo, Voltas, & Ferrio, 2015).

487

488 *Strengthening of $\Delta^{13}C$ -growth relationships in response to climate change*

489 The geographical structure of tree growth relationships with carbon isotope fractionation
490 processes varied during the 20th century. Alongside the increase in growth synchrony observed
491 at the temperate, cold-continental and Mediterranean groups, a change from non-significant to
492 positive correlations suggests intensified drought impacts on tree physiology since 1950 (Saurer
493 et al., 2014). Such warming-induced drought effects influencing stomatal regulation have been
494 shown insufficient to decrease 20th-century transpiration, as alternative factors (e.g., lengthened
495 growing seasons or increased leaf area) counterbalance the impacts of leaf-level gas exchange

496 processes on whole-tree physiology (Frank et al., 2015). Indeed, we found evidence of growth
497 enhancement across Europe, but mainly in oaks originating from moist temperate climates in
498 low-elevation stands. For conifers, growth stimulation was observed in some of the cold-limited
499 sites, while growth decline was found in drought-constrained Mediterranean mountains. In
500 high-latitude and high-elevation sites, the increasing growth trend could be produced by a raise
501 in photosynthetic rates, which is likely driven by a combination of rising CO₂, temperature and
502 surface radiation. However, drought stress seems to override a positive effect of enhanced leaf
503 intercellular CO₂ concentration in the Mediterranean region, resulting in no change or decline
504 in productivity (Andreu-Hayles et al., 2011).

505 In Fennoscandia, the negative ring-width dependence on $\Delta^{13}\text{C}$ vanished after 1950,
506 which suggests that an earlier photosynthetic limitation of growth driven by low temperatures,
507 high cloudiness or both factors has attenuated in recent decades. In the western Mediterranean,
508 this dependence changed abruptly from zero to nearly one after 1970. Previously, growth
509 synchrony among the group chronologies was absent, rendering a null signal shared by ring-
510 width and $\Delta^{13}\text{C}$. After 1950, a common growth signal was low but relevant: this signal was
511 essentially related to $\Delta^{13}\text{C}$ fluctuations, resulting in a highly positive correlation. Although this
512 correlation implies a tight stomatal control of common radial growth in high-mountain
513 Mediterranean forests, the limited number of chronologies and the sudden change in tree
514 performance between periods might question this interpretation. A recent study carried out in
515 Iberian mountain forests allows the downscaling of our results to a local area (Shestakova et
516 al., 2017). These authors reported that multispecies tree growth at about 1,500 m is more
517 dependent on a tighter stomatal control of water losses (inferred from $\Delta^{13}\text{C}$) since the 1980s,
518 hence resembling lower elevation stands. These results reinforce our view, although more data
519 supporting this evidence are still needed on a regional scale. Unfortunately, studies on long-
520 term shifts in radial growth related to switches of the main environmental limitations to
521 photosynthetic carbon gain are still scarce (Voelker et al., 2014).

522 To conclude, we have reported forest shifts from temperature- to moisture-sensitive
523 growth spreading northwards continent-wide and associated to latitudinal changes in tree
524 dependence on carbon isotope fractionation processes. Leaf-level physiology and radial growth
525 of trees are ultimately linked via carbon allocation strategies. Common signals imprinted in
526 ring-width and stable isotopes have been broadly reported, either along geographical gradients
527 (i.e., phenotypic plasticity; del Castillo et al., 2015), over time (i.e., temporal covariation;
528 Voelker et al., 2014; Shestakova et al., 2017; this work) or at the intraspecific level (i.e., genetic
529 correlation; Fardusi et al., 2016). These evidences support (direct or indirect) effects of carbon

530 uptake processes on above-ground growth. On the other hand, carbohydrates are used for
531 various other processes than growth (e.g., maintenance, respiration, reproduction) and carbon
532 availability is seldom considered to limit tree growth (Palacio, Hoch, Sala, Körner, & Millard,
533 2014; but see Wiley & Helliker, 2012), which suggests that the relationship between
534 productivity and stable isotopes may not be straightforward (Jucker et al., 2017). Alternative
535 physiological mechanisms related to above-ground growth may interact with photosynthetic
536 processes; for example, a critical turgor disrupting cell growth or the appearance of hydraulic
537 constraints under drought (Sperry, 2000), or the weakening of meristematic growth under low
538 temperatures (Rossi et al., 2016). These mechanisms would need to be carefully assessed
539 against stable isotope signals.

540 Together with climate change, the increasing atmCO_2 may have played a role in the
541 observed shift in growth synchrony and the stronger relation between $\Delta^{13}\text{C}$ and TRW_i .
542 Disentangling the relative effects of climate and CO_2 fertilization on spatially structured tree-
543 ring information is challenging because both low- and high-frequency signals overlap
544 impacting on tree physiology, carbon allocation and above- and below-ground growth.
545 Additional factors interacting with climate change and atmCO_2 such as increasing nutrient
546 limitations (Jonard et al., 2015) or atmospheric deposition (de Vries, Dobbertin, Solberg, van
547 Dobben, & Schaub, 2014) should also be considered. A previous study on the same tree-ring
548 network demonstrated that CO_2 fertilization has increased water-use efficiency of European
549 forests in the 20th century (Saurer et al., 2014). However, these increments were not spatially
550 uniform and, notably, the strongest increase was reported in response to summer drought for
551 temperate forests in central Europe, an area in which we observe large increases in growth
552 synchrony. These findings definitely point to an increasing impact of water stress spreading
553 northwards across European forests. Therefore, this research demonstrates that broad-scale
554 climatic variation jointly influences tree ecophysiology and productivity in previously
555 unrecognized ways, and sheds more light on the ecological implications of ecosystem
556 functioning under the new climate conditions.

557 **References**

- 558 Anderegg, W. R. L., Klein, T., Barlett, M., Sack, L., Pellegrini, A.F., Choat, B., & Jansen, S.
559 (2016). Meta-analysis reveals that hydraulic traits explain cross-species patterns of
560 drought-induced tree mortality across the globe. *Proceedings of the National Academy
561 of Sciences of the United States of America*, **113**, 5024–5029.
- 562 Andreu-Hayles, L., Gutiérrez, E., Muntan, E., Helle, G., Anchukaitis, K. J., & Schleser, G. H.
563 (2011). Long tree-ring chronologies reveal 20th century increases in water-use efficiency
564 but no enhancement of tree growth at five Iberian pine forests. *Global Change Biology*,
565 **17**, 2095–2112.
- 566 Babst, F., Poulter, B., Trouet, V., Tan, K., Neuwirth, B., Wilson, R., Carrer, M., Grabner, M.,
567 Tegel, W., Levanič, T., Panayotov, M., Urbinati, C., Bouriaud, O., Ciais, P., & Frank,
568 D. (2013). Site- and species-specific responses of forest growth to climate across the
569 European continent. *Global Ecology and Biogeography*, **22**, 706–717.
- 570 Burnham, K.P., & Anderson, D.R. (2002) *Model selection and multi-model inference: A
571 practical information – theoretic approach*. Springer, New York 488 pp.
- 572 Cernusak, L. A., & English, N. B. (2015). Beyond tree-ring widths: stable isotopes sharpen the
573 focus of climate response of temperate forest trees. *Tree Physiology*, **35**, 1–3.
- 574 Chown, S. L., Gaston, K. J., & Robinson, D. (2004). Macrophysiology: large-scale patterns in
575 physiological traits and their ecological implications. *Functional Ecology*, **18**, 159–167.
- 576 Cook, E. R., & Kairiukstis, L. A. (1990). *Methods of dendrochronology: Applications in the
577 environmental sciences*. Dordrecht, Netherlands: Springer Netherlands.
- 578 Cullen, L. E., Adams, M. A., Anderson, M. J., & Grierson, P. F. (2008). Analyses of $\delta^{13}\text{C}$ and
579 $\delta^{18}\text{O}$ in tree rings of *Callitris columellaris* provide evidence of a change in stomatal
580 control of photosynthesis in response to regional changes in climate. *Tree Physiology*,
581 **28**, 1525–1533.
- 582 de Vries, W., Dobbertin, M. H., Solberg, H., van Dobben, H. F., & Schaub, M. (2014). Impacts
583 of acid deposition, ozone exposure and weather conditions on forest ecosystems in
584 Europe: an overview. *Plant and Soil*, **380**, 1–45.
- 585 del Castillo, J., Voltas, J., & Ferrio, J. P. (2015). Carbon isotope discrimination, radial growth,
586 and NDVI share spatiotemporal responses to precipitation in Aleppo pine. *Trees*, **29**,
587 223–233.
- 588 DÜthorn, E., Schneider, L., Günther, B., Gläser, S., & Esper, J. (2016). Ecological and
589 climatological signals in tree-ring width and density chronologies along a latitudinal
590 boreal transect. *Scandinavian Journal of Forest Research*, **31**, 750–757.

591 European Environment Agency (2016). *Trends in annual temperature across Europe between*
592 *1960 and 2015*. [WWW document] URL [http://www.eea.europa.eu/data-and-](http://www.eea.europa.eu/data-and-maps/figures/decadal-average-trends-in-mean-6)
593 [maps/figures/decadal-average-trends-in-mean-6](http://www.eea.europa.eu/data-and-maps/figures/decadal-average-trends-in-mean-6). [accessed 1 August 2018].

594 Fardusi, M. S., Ferrio, J. P., Comas, C., Voltas, J., Resco de Dios, V., & Serrano, L. (2016).
595 Intra-specific association between carbon isotope composition and productivity in
596 woody plants: a meta-analysis. *Plant Science*, **251**, 110–118.

597 Farquhar, G. D., Ehleringer, J. R., & Hubick, K. T. (1989). Carbon isotope discrimination and
598 photosynthesis. *Annual Review of Plant Physiology and Plant Molecular Biology*, **40**,
599 503–537.

600 Frank, D. C., Poulter, B., Saurer, M., Esper, J., Huntingford, C., Helle, G., Treydte, K.,
601 Zimmermann, N. E., Schleser, G. H., Ahlström, A., Ciais, P., Friedlingstein, P., Levis,
602 S., Lomas, M., Sitch, S., Viovy, N., Andreu-Hayles, L., Bednarz, Z., Berninger, F.,
603 Boettger, T., D'Alessandro, C. M., Daux, V., Filot, M., Grabner, M., Gutierrez, E.,
604 Haupt, M., Hilasvuori, E., Jungner, H., Kalela-Brundin, M., Krapiec, M., Leuenberger,
605 M., Loader, N. J., Marah, H., Masson-Delmotte, V., Pazdur, A., Pawelczyk, S., Pierre,
606 M., Planells, O., Pukiene, R., Reynolds-Henne, C. E., Rinne, K. T., Saracino, A.,
607 Sonninen, E., Stievenard, M., Switsur, V. R., Szczepanek, M., Szychowska-Krapiec, E.,
608 Todaro, L., Waterhouse, J. S., & Weigl, M. (2015). Water-use efficiency and
609 transpiration across European forests during the Anthropocene. *Nature Climate Change*,
610 **5**, 579–584.

611 Fritts, H. C. (2001). *Tree rings and climate*. Caldwell, NJ: Blackburn Press.

612 Gagen, M., Zorita, E., McCarroll, D., Young, G. H. F., Grudd, H., Jalkanen, R., Loader, N. J.,
613 Robertson, I., & Kirchhefer, A. (2011). Cloud response to summer temperatures in
614 Fennoscandia over the last thousand years. *Geophysical Research Letters*, **38**, L05701.

615 Gandullo, J. M. (1994). *Climatología y ciencia del suelo*. Madrid, Spain: Fundación Conde del
616 Valle de Salazar.

617 Gessler, A., Ferrio, J. P., Hommel, R., Treydte, K., Werner, R., & Monson, R. K. (2014). Stable
618 isotopes in tree rings: toward a mechanistic understanding of fractionation and mixing
619 processes from the leaves to the wood. *Tree Physiology*, **34**, 796–818.

620 Gibert, A., Gray, E. F., Westoby, M., Wright, I. J., & Falster, D. S. (2016). On the link between
621 functional traits and growth rate: meta-analysis shows effects change with plant size, as
622 predicted. *Journal of Ecology*, **104**, 1488–1503.

623 Grissino-Mayer, H. D, & Fritts, H. C. (1997). The International Tree-Ring Data Bank: an
624 enhanced global database serving the global scientific community. *Holocene*, **7**, 235–
625 228.

626 Hamed, K. H., & Rao, A. R. (1998). A modified Mann Kendall trend test for autocorrelated
627 data. *Journal of Hydrology*, **204**, 182–196.

628 Hargreaves, G. H., & Samani, Z.A. (1982). Estimating potential evapotranspiration. *Journal of*
629 *the Irrigation & Drainage Division – ASCE*, **108**, 225–230.

630 Harris, I., Jones, P. D., Osborn, T. J., & Lister, D. H. (2014). Updated high-resolution grids of
631 monthly climatic observations – the CRU TS3.10 Dataset. *International Journal of*
632 *Climatology*, **34**, 623–642.

633 Hartl-Meier, C., Zang, C., Büntgen, U., Esper, J., Rothe, A., Göttelein, A., Dirnböck, T., &
634 Treydte, K. (2015). Uniform climate sensitivity in tree-ring stable isotopes across
635 species and sites in a mid-latitude temperate forest. *Tree Physiology*, **35**, 4–15.

636 Jonard, M., Fürst, A., Verstraeten, A., Thimonier, A., Timmermann, V., Potočić, N., Waldner,
637 P., Benham, S., Hansen, K., Merilä, P., Ponette, Q., de la Cruz, A. C., Roskams, P.,
638 Nicolas, M., Croisé, L., Ingerslev, M., Matteucci, G., Decinti, B., Bascietto, M., &
639 Rautio, P. (2015). Tree mineral nutrition is deteriorating in Europe. *Global Change*
640 *Biology*, **21**, 418–430.

641 Jones, H. G. (1992). *Plants and microclimate*. Cambridge, England: Cambridge University
642 Press.

643 Jucker, T., Grossiord, C., Bonal, D., Bouriaud, O., Gessler, A., & Coomes, D. A. (2017).
644 Detecting the fingerprint of drought across Europe’s forests: do carbon isotope ratios
645 and stem growth rates tell similar stories? *Forest Ecosystems*, **4**, 24.

646 Köppen, W., & Geiger, R. (1936). *Handbuch der klimatologie*. Berlin, Germany: Gebrüder
647 Bornträger.

648 Koenig, W. D., & Knops, J. M. H. (1998). Testing for spatial autocorrelation in ecological
649 studies. *Ecography*, **21**, 423–429.

650 Kress, A., Young, G. H. F., Saurer, M., Loader, N. J., Siegwolf, R. T. W., & McCarroll, D.
651 (2009). Stable isotope coherence in the earlywood and latewood of tree-line conifers.
652 *Chemical Geology*, **268**, 52–57.

653 Latte, N., Lebourgeois, F., & Claessens, H. (2015). Increased tree-growth synchronization of
654 beech (*Fagus sylvatica* L.) in response to climate change in northwestern Europe.
655 *Dendrochronologia*, **33**, 69–77.

656 Livingston, N.J., Whitehead, D., Kelliher, F.M., Wang, Y.P., Grace, J.C., Walcroft, A.S., Byers,
657 J.N., McSeveny, T.M. & Millard, P. (1998) Nitrogen allocation and carbon isotope
658 fractionation in relation to intercepted radiation and position in a young *Pinus radiata*
659 D. Don tree. *Plant, Cell & Environment*, **21**, 795–803.

660 Nabuurs, G. J., Lindner, M., Verkerk, P. J., Gunia, K., Deda, P., Michalak, R., & Grassi, G.
661 (2013). First signs of carbon sink saturation in European forest biomass. *Nature Climate*
662 *Change*, **3**, 792–796.

663 Orłowsky, B., & Seneviratne, S. I. (2014). On the spatial representativeness of temporal
664 dynamics at European weather stations. *International Journal of Climatology*, **34**,
665 3154–3160.

666 Palacio, S., Hoch, G., Sala, A., Körner, C., & Millard, P. (2014). Does carbon storage limit tree
667 growth? *New Phytologist*, **201**, 1096–1100.

668 Pivovarov, A. L., Pasquini, S. C., De Guzman, M. E., Alstad, K. P., Stemke, J. S., & Santiago,
669 L. S. (2016). Multiple strategies for drought survival among woody plant species.
670 *Functional Ecology*, **30**, 517–526.

671 Rossi, S., Anfodillo, T., Čufar, K., Cuny, H. E., Deslauriers, A., Fonti, P., Frank, D., Gričar, J.,
672 Gruber, A., Huang, J. G., Jyske, T., Kašpar, J., King, G., Krause, C., Liang, E., Mäkinen,
673 H., Morin, H., Nöjd, P., Oberhuber, W., Prislán, P., Rathgeber, C. B., Saracino, A.,
674 Swidrak, I., & Treml, V. (2016). Pattern of xylem phenology in conifers of cold forest
675 ecosystems at the Northern Hemisphere. *Global Change Biology*, **22**, 3804–3813.

676 Saurer, M., Spahni, R., Frank, D. C., Joos, F., Leuenberger, M., Loader, N. J., McCarroll, D.,
677 Gagen, M., Poulter, B., Siegwolf, R. T. W., Andreu-Hayles, L., Boettger, T., Dorado
678 Liñán, I., Fairchild, I. J., Friedrich, M., Gutiérrez, E., Haupt, M., Hiltunen, E.,
679 Heinrich, I., Helle, G., Grudd, H., Jalkanen, R., Levanič, T., Linderholm, H. W.,
680 Robertson, I., Sonninen, E., Treydte, K., Waterhouse, J. S., Woodley, E. J., Wynn, P.
681 M., & Young, G. H. (2014). Spatial variability and temporal trends in water-use
682 efficiency of European forest. *Global Change Biology*, **20**, 332–336.

683 Shestakova, T. A., Aguilera, M., Ferrio, J. P., Gutiérrez, E., & Voltas, J. (2014). Unravelling
684 spatiotemporal tree-ring signals in Mediterranean oaks: a variance–covariance
685 modelling approach of carbon and oxygen isotope ratios. *Tree Physiology*, **34**, 819–838.

686 Shestakova, T. A., Gutiérrez, E., Kirilyanov, A. V., Camarero, J. J., Génova, M., Knorre, A. A.,
687 Linares, J. C., Resco de Dios, V., Sánchez-Salguero, R., & Voltas, J. (2016). Forests
688 synchronize their growth in contrasting Eurasian regions in response to climate

689 warming. *Proceedings of the National Academy of Sciences of the United States of*
690 *America*, **113**, 662–667.

691 Shestakova, T. A., Camarero, J. J., Ferrio, J. P., Knorre, A. A., Gutiérrez, E., & Voltas, J. (2017).
692 Increasing drought effects on five European pines modulate $\Delta^{13}\text{C}$ -growth coupling
693 along a Mediterranean altitudinal gradient. *Functional Ecology*, **31**, 1359–1370.

694 Shestakova, T. A., Gutiérrez, E., & Voltas, J. (2018). A roadmap to disentangling
695 ecogeographical patterns of spatial synchrony in dendrosciences. *Trees*, **32**, 359–370.

696 Sperry, J. S. (2000). Hydraulic constraints on plant gas exchange. *Agricultural and Forest*
697 *Meteorology*, **104**, 13–23.

698 Stuiver, M., & Braziunas, T. F. (1987). Tree cellulose $^{13}\text{C}/^{12}\text{C}$ isotope ratios and climatic
699 change. *Nature*, **328**, 58–60.

700 Treydte, K., Frank, D. C., Esper, J., Andreu, L., Bednarz, Z., Berninger, F., Boettger, T.,
701 D'Alessandro, C. M., Etien, N., Filot, M., Grabner, M., Guillemain, M. T., Gutierrez, E.,
702 Haupt, M., Helle, G., Hilasvuori, E., Jungner, H., Kalela-Brundin, M., Krapiec, M.,
703 Leuenberger, M., Loader, N. J., Masson-Delmotte, V., Pazdur, A., Pawelczyk, S.,
704 Pierre, M., Planells, O., Pukiene, R., Reynolds-Henne, C. E., Rinne, K. T., Saracino, A.,
705 Saurer, M., Sonninen, E., Stievenard, M., Switsur, V. R., Szczepanek, M., Szychowska-
706 Krapiec, E., Todaro, L., Waterhouse, J. S., Weigl, M., & Schleser, G. H. (2007). Signal
707 strength and climate calibration of a European tree-ring isotope network. *Geophysical*
708 *Research Letters*, **34**, L24302.

709 Vicente-Serrano, S. M., Beguería, S., & López-Moreno, J. I. (2010). A Multiscalar drought
710 index sensitive to global warming: the Standardized Precipitation Evapotranspiration
711 Index. *Journal of Climate*, **23**, 1696–1718.

712 Violle, C., Reich, P. B., Pacala, S. W., Enquist, B. J., & Kattge, J. (2014). The emergence and
713 promise of functional biogeography. *Proceedings of the National Academy of Sciences*
714 *of the United States of America*, **111**, 13690–13696.

715 Voelker, S. L., Meinzer, F. C., Lachenbruch, B., Brooks, J. R., & Guyette, R. P. (2014). Drivers
716 of radial growth and carbon isotope discrimination of bur oak (*Quercus macrocarpa*
717 Michx.) across continental gradients in precipitation, vapour pressure deficit and
718 irradiance. *Plant, Cell and Environment*, **37**, 766–779.

719 Way, D. A., & Oren, R. (2010). Differential responses to changes in growth temperature
720 between trees from different functional groups and biomes: a review and synthesis of
721 data. *Tree Physiology*, **30**, 669–688.

722 Werner, C., Schnyder, H., Cuntz, M., Keitel, C., Zeeman, M. J., Dawson, T. E., Badeck, F. W.,
723 Brugnoli, E., Ghashghaie, J., Grams, T. E. E., Kayler, Z. E., Lakatos, M., Lee, X.,
724 Maguas, C., Ogee, J., Rascher, K. G., Siegwolf, R. T. W., Unger, S., Welker, J.,
725 Wingate, L., & Gessler, A. (2012). Progress and challenges in using stable isotopes to
726 trace plant carbon and water relations across scales. *Biogeosciences*, **9**, 3083–3111.
727 Wiley, E. & Helliker, B. (2012). A re-evaluation of carbon storage in trees lends greater support
728 for carbon limitation to growth. *New Phytologist*, **195**, 285-289.

729

730 **Data Accessibility Statement**

731 The tree-ring data used in this study are available upon request from the authors. Contact Emilia
732 Gutiérrez (emgutierrez@ub.edu) for ring-width chronologies and Gerhard Helle ([ghelle@gfz-](mailto:ghelle@gfz-potsdam.de)
733 [potsdam.de](http://gfz-potsdam.de)) for carbon isotope records.

734

735 **Biosketch**

736 Tatiana A. Shestakova is a post-doctoral researcher at the Woods Hole Research Center,
737 Falmouth, MA (USA). Her research interests include dendroecology, stable isotope
738 biogeochemistry and climate change impacts on natural forest ecosystem. Particularly, she
739 works on designing efficient inference tools and algorithms based on mixed modelling
740 principles to understand the processes underlying the complexity and diversity in tree response
741 patterns to environmental forcing and how these patterns are spatially structured across
742 biogeographical gradients.

743

744 **FIGURE CAPTIONS**

745

746 Figure 1. Spatial patterns of indexed tree-ring traits across Europe for the period 1901–2003:
747 **(a, c)** indexed tree-ring width (TRW_i), **(b, d)** indexed carbon isotope discrimination ($\Delta^{13}\text{C}_i$).
748 *(Left panels)* Pairwise correlations of tree-ring chronologies as a function of geographical
749 distance. The patterns are summarized by regressing the correlation coefficients (r values)
750 involving pairs of chronologies (y -axis) on their corresponding distance (x -axis) by using
751 negative exponential functions ($y = be^{-cx}$). Different dot colors indicate pairwise correlations
752 within and between functional groups as follows: conifers (green), oaks (orange), and mixed
753 conifer–oak (blue). Asterisks after the coefficient of determination (r^2) indicate level of
754 significance ($***P < 0.001$). *(Right panels)* Spatial structure of tree-ring traits across European
755 forests. The spatial autocorrelation in the tree-ring network was characterized for six
756 consecutive distance classes (listed on the x -axis). Mean r values and their statistical
757 significance (P) within each distance class were estimated from 1,000 randomizations.
758 Significant correlation coefficients ($P < 0.05$) are indicated by an asterisk.

759

760 Figure 2. Geographical distribution of sites, definition of groups of chronologies and synchrony
761 in radial growth at group level. Each dot identifies a chronology ($n \geq 20$ trees) according to the
762 codes shown in Table 1 (oak codes are shown in italics). Each colored encircled area identifies
763 a group of chronologies belonging to a particular climate type (see Table 1) that are separated
764 in pairs up to 1,000 km (see Fig. 1d for the distance threshold where significant radial growth
765 patterns are shared among chronologies). The corresponding growth synchrony at the group
766 level (\hat{a}) is shown within a rectangle. At least three neighbouring sites form a group (total
767 number of groups, $n = 5$). \hat{a} values are estimated using indexed ring-width chronologies for the
768 period 1901–2003 as described in Appendix 3.1 (Supporting Information).

769

770 Figure 3. Growth synchrony across Europe. Patterns of growth synchrony (\hat{a}) at the within-
771 group level for the entire period 1901–2003 **(a)**. Patterns of growth synchrony (\hat{a}) at the
772 between-group level for the entire period 1901–2003 **(b)**. All calculations are based on indexed
773 ring-width chronologies. Groups sorted latitudinally from north to south. Error bars denote
774 standard errors.

775

776 Figure 4. Temporal trends in growth synchrony at within- and between-group levels for the
777 period 1901–2003. Growth synchrony (\hat{a}) is estimated for 50-year periods lagged by 5 year

778 following Eqs. 5 and 6 as described in Appendix 3.1 (Supporting Information). All calculations
779 are based on indexed ring-width (TRW_i) chronologies. For the sake of visual clarity, the
780 estimates of \hat{a} are represented separately for pairs of chronologies belonging to the same group
781 (i.e., within-group level) **(a)**, and for pairs of chronologies belonging to different groups (i.e.,
782 between-group level) for neighbouring **(b)** and non-neighbouring chronologies **(c)**. Grey lines
783 denote the SE. Note the change in scale of the Y-axis between panels.

784

785 Figure 5. Geographical patterns of the relationship between TRW_i and $\Delta^{13}C_i$ chronologies
786 across Europe. The correlations at the group level (r_Y) are estimated for the entire period 1901–
787 2003. Significant associations are depicted with an asterisk ($P < 0.10$). Error bars denote
788 standard errors.

789

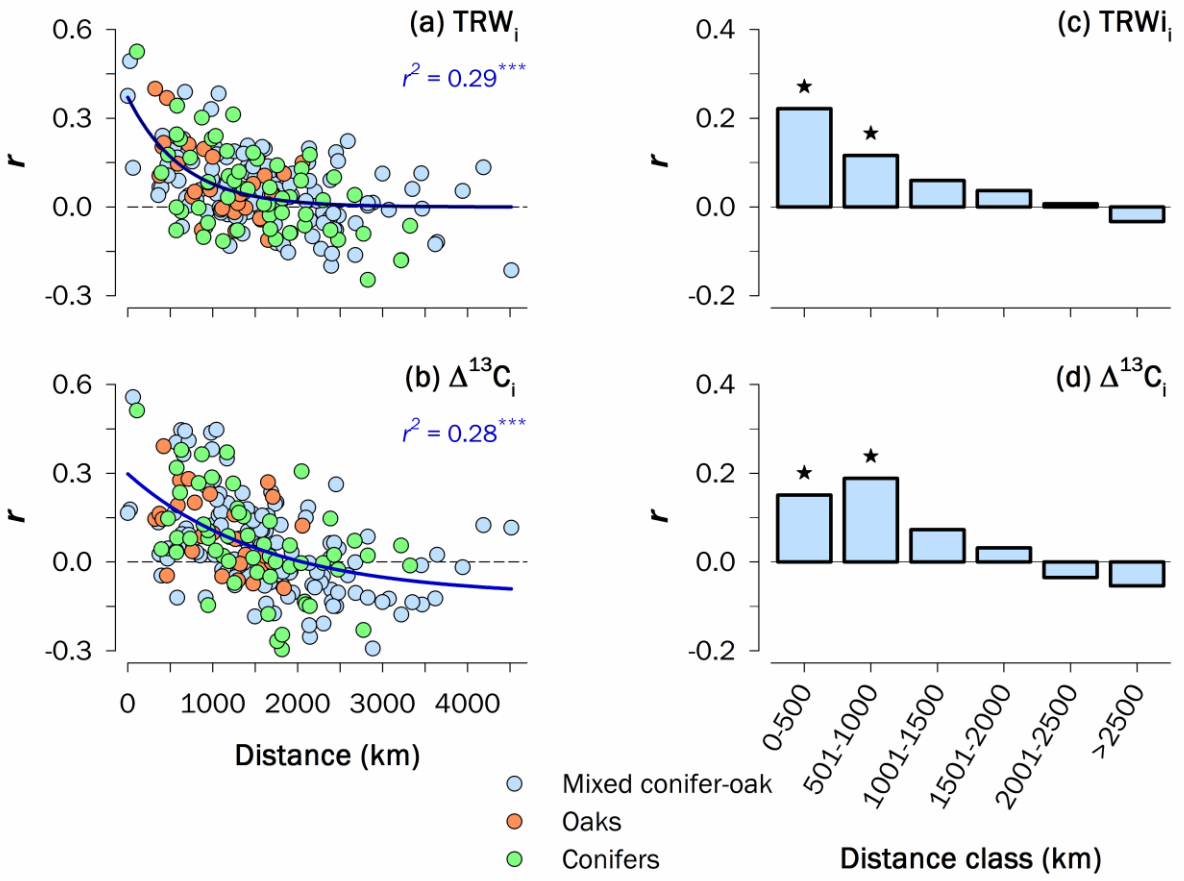
790 Figure 6. Temporal trends in associations between TRW_i and $\Delta^{13}C_i$ chronologies at the group
791 level for the period 1901–2003. The correlations (r_Y) are estimated for 50-year periods lagged
792 by 5 year following Eq. 7 as described in Appendix 3.2 (Supporting Information). All
793 calculations are based on indexed ring-width (TRW_i) and carbon isotope ($\Delta^{13}C_i$) chronologies.
794 Grey lines denote the SE of r_Y . Significant correlations (correlation coefficients with 90%
795 confidence intervals not embracing zero) are depicted as filled dots.

796

797 **Table 1.** Geographical features and climatic characteristics of the sampling sites. Sites are sorted latitudinally
798 Climate parameters were obtained based on CRU TS 3.21 data over the period 1901–2003. See Meteorology
799 Methods for details. Climate types were estimated using the Köppen classification (Köppen & Geiger, 1936).

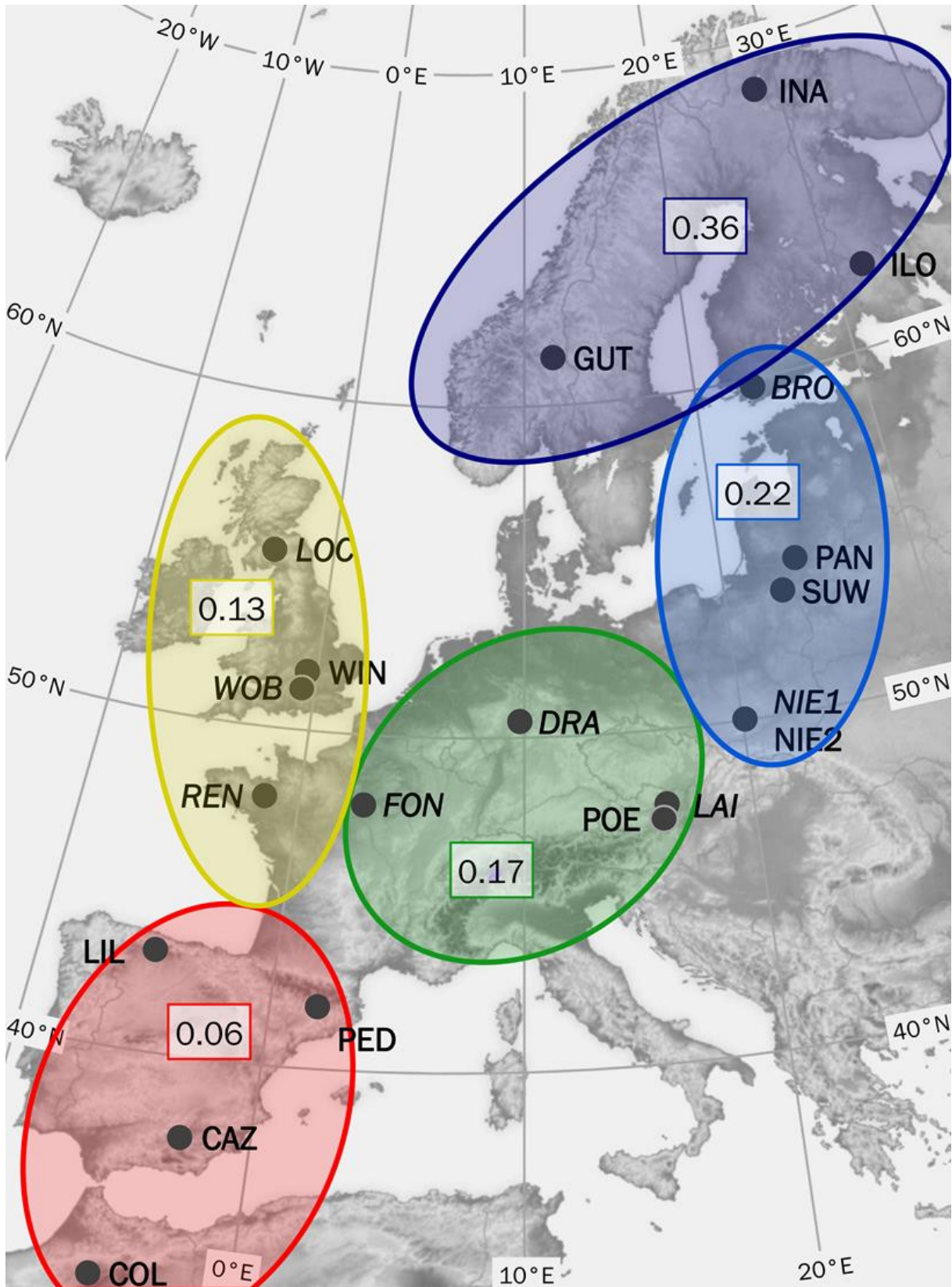
No	Country	Site name	Code	Species	Latitude (°N)	Longitude (°E)	Elevation (m)	MAT (°C)	MAP (mm)	PET (mm)	MA
1	Finland	Kessi, Inari	INA	<i>Pinus sylvestris</i>	68.93	28.42	150	−1.2	432	413	Ap
2	Finland	Sivak., Ilomantsi	ILO	<i>Pinus sylvestris</i>	62.98	31.27	200	2.2	573	515	Ap
3	Norway	Gutuli	GUT	<i>Pinus sylvestris</i>	62.00	12.18	800	0.7	586	512	Ap
4	Finland	Bromarv	BRO	<i>Quercus robur</i>	60.00	23.08	5	4.9	568	562	Ap
5	UK	Lochwood	LOC	<i>Quercus robur</i>	55.27	−3.43	175	7.4	1517	589	
6	Lithuania	Panemunės Silas	PAN	<i>Pinus sylvestris</i>	54.88	23.97	45	6.6	634	672	A
7	Poland	Suwalki	SUW	<i>Pinus sylvestris</i>	54.10	22.93	160	6.7	619	686	A
8	UK	Woburn Abbey	WOB	<i>Quercus robur</i>	51.98	−0.59	50	9.5	709	724	A
9	Germany	Dransfeld	DRA	<i>Quercus petraea</i>	51.50	9.78	320	7.7	723	677	A
10	UK	Windsor	WIN	<i>Pinus sylvestris</i>	51.41	−0.59	10	9.5	763	738	A
11	Poland	Niepolomice, Gibiel	NIE1	<i>Quercus robur</i>	50.12	20.38	190	8.0	676	674	Ap
12	Poland	Niepolomice, Gibiel	NIE2	<i>Pinus sylvestris</i>	50.12	20.38	190	8.0	676	674	Ap
13	France	Fontainebleau	FON	<i>Quercus petraea</i>	48.38	2.67	100	11.5	608	861	M
14	France	Rennes	REN	<i>Quercus robur</i>	48.25	−1.70	100	11.1	733	786	A
15	Austria	Lainzer Tiergarten	LAI	<i>Quercus petraea</i>	48.18	16.20	300	9.6	654	792	M
16	Austria	Poellau	POE	<i>Pinus nigra</i>	47.95	16.06	500	8.3	815	762	Ap
17	Spain	Pinar de Lillo	LIL	<i>Pinus sylvestris</i>	43.07	−5.25	1600	5.1	1505	688	Ju
28	Spain	Massis de Pedraforca	PED	<i>Pinus uncinata</i>	42.23	1.70	2100	3.9	1299	692	Ju
19	Spain	Sierra de Cazorla	CAZ	<i>Pinus nigra</i>	37.80	−2.95	1816	8.9	712	1014	M
20	Morocco	Col du Zad	COL	<i>Cedrus atlantica</i>	32.97	−5.07	2200	10.4	717	1163	A

800 Abbreviations: MAT, mean annual temperature; MAP, mean annual precipitation; PET, potential evapotranspiration; BAI, basal area
801 * $P < 0.05$; ** $P < 0.01$; *** $P < 0.001$. The significance of BAI trends is assessed using the Mann-Kendall non-parametric test which accounts for
802 autocorrelation (Hamed & Rao, 1998)



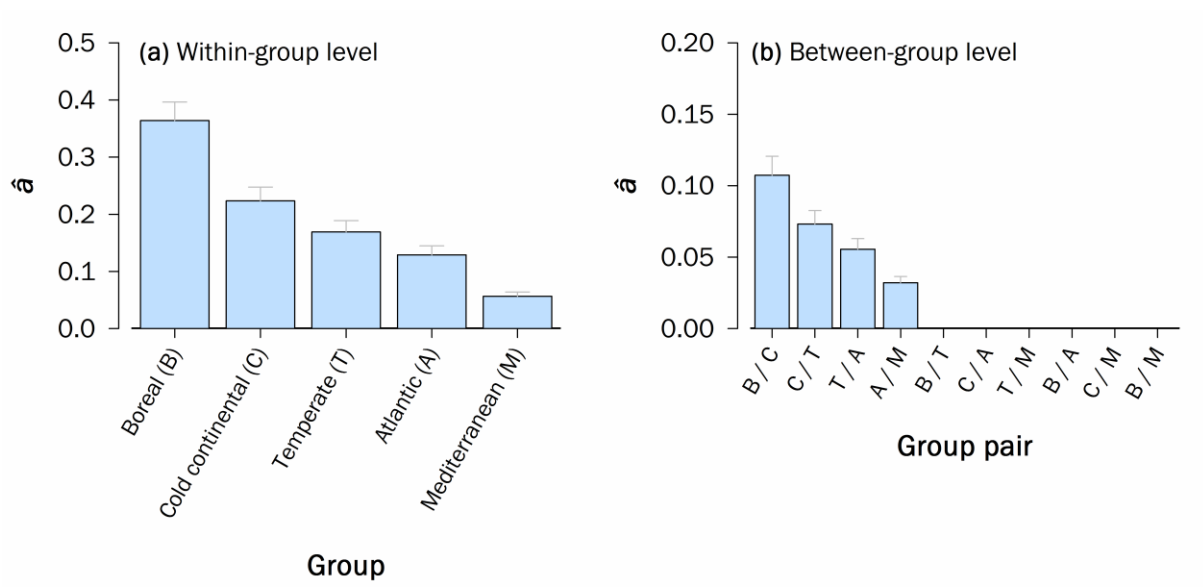
803

804 **Figure 1**



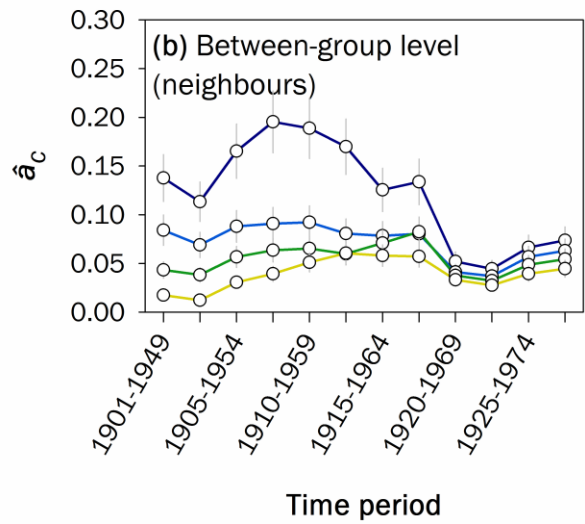
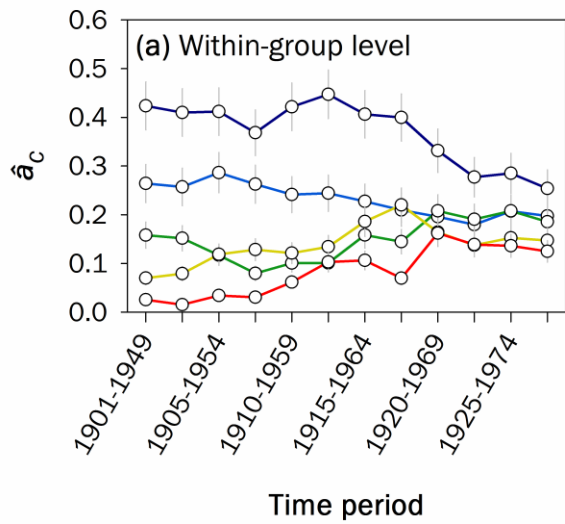
805

806 **Figure 2**



807

808 **Figure 3**

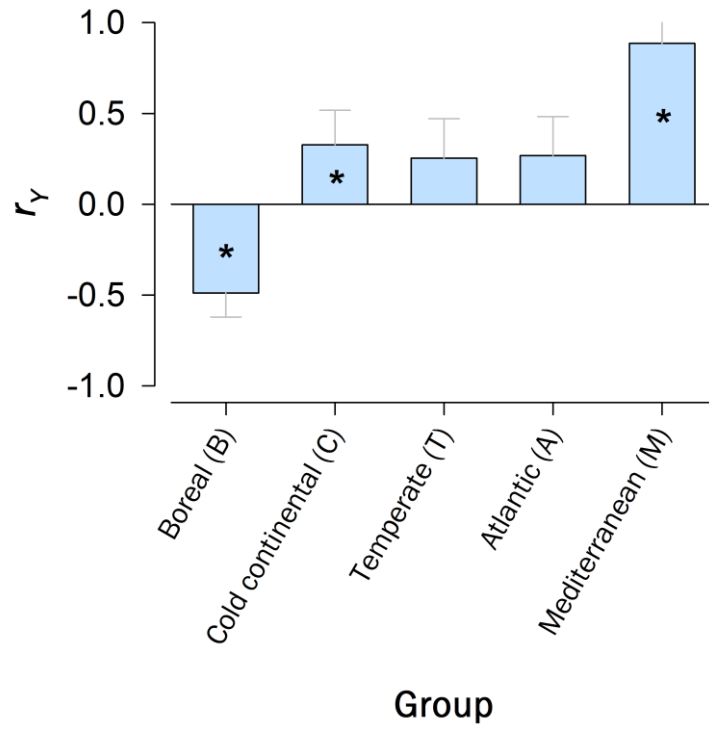


- Boreal (B)
- Cold continental (CC)
- Temperate (T)
- Atlantic (A)
- Mediterranean (M)

- B/CC
- CC/T
- T/A
- A/M

809

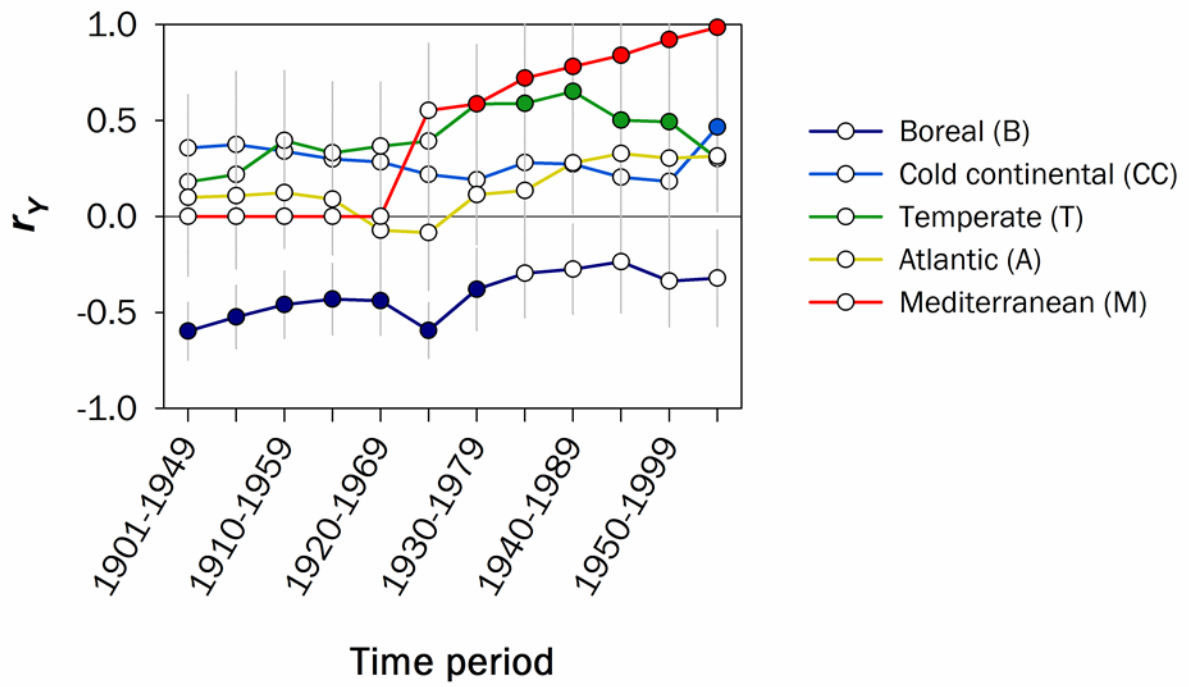
810 **Figure 4**



811

812 **Figure 5**

813



814

815 **Figure 6**

816 **Supporting Information**

817

818 Additional Supporting Information may be found in the online version of this article:

819 **Appendix 1.** Field sampling and tree-ring measurements.

820 **Appendix 2.** Tree-ring chronology characteristics.

821 **Appendix 3.** Random modelling analysis.

822 **Appendix 4.** Further evaluation of geographical trends in growth synchrony across Europe.

823 **Table S1.** Dendrochronological characteristics of the study sites.

824 **Table S2.** Description of variance-covariance (VCOV) models accommodating between- and
825 within-group variability.

826 **Table S3.** Results of variance-covariance models for synchrony analysis.

827 **Figure S1.** Climate signals at the site level for TRW_i and $\Delta^{13}C_i$ for the period 1901–2003.

828 **Figure S2.** Principal component analysis performed on 20 indexed ring-width chronologies
829 distributed across Europe and northern Africa for the common period 1901–1998.

830 **Figure S3.** Spatial patterns of climate signals (mean annual temperature, MAT; mean annual
831 precipitation, MAP) across Europe for the period 1901–2003.

832 **Figure S4.** Geographical patterns of growth synchrony (\hat{a}) at the group level for the entire
833 period 1901–2003 and change in \hat{a} for two consecutive periods (1901–1950 and 1951–2003).

834 **Figure S5.** Geographical patterns of growth synchrony (\hat{a}) for chronologies obtained from the
835 International Tree-Ring Data Bank (ITRDB) dataset for the period 1901–2003.

836 **Figure S6.** Climatic patterns of growth synchrony (\hat{a}) at the group level for the entire period
837 1901–2003 and change in \hat{a} for two consecutive periods (1901–1950 and 1951–2003).

838 **Figure S7.** Geographical patterns of the relationship between TRW_i and $\Delta^{13}C_i$ chronologies
839 across Europe for the entire period 1901–2003 and for two consecutive periods (1901–1950
840 and 1951–2003).

841 **Figure S8.** Climatic patterns of the relationship between TRW_i and $\Delta^{13}C_i$ chronologies across
842 Europe for the entire period 1901–2003 and for two consecutive periods (1901–1950 and
843 1951–2003).

844 **Figure S9.** Trends in climate parameters: mean annual temperature (MAT) and mean annual
845 precipitation (MAP) at the group level.